

# Study of amyloid- $\beta$ peptide functional brain networks in AD, MCI and HC<sup>1</sup>

Jiehui Jiang<sup>a</sup>, Huoqiang Duan<sup>a</sup>, Zheming Huang<sup>b</sup>, Zhihua Yu<sup>c,\*</sup> and The Alzheimer's Disease Neuroimaging Initiative<sup>2</sup>

<sup>a</sup>*Institute of Biomedical Engineering, School of Communication and Information Technology, Shanghai University, Shanghai, China*

<sup>b</sup>*PET Center, Huashan Hospital, Fudan University, Shanghai, China*

<sup>c</sup>*Shanghai Geriatric Institute of Chinese Medicine, Shanghai, China*

**Abstract.** One medical challenge in studying the amyloid- $\beta$  (A $\beta$ ) peptide mechanism for Alzheimer's disease (AD) is exploring the law of beta toxic oligomers' diffusion in human brains *in vivo*. One beneficial means of solving this problem is brain network analysis based on graph theory. In this study, the characteristics of A $\beta$  functional brain networks of Healthy Control (HC), Mild Cognitive Impairment (MCI), and AD groups were compared by applying graph theoretical analyses to Carbon 11-labeled Pittsburgh compound B positron emission tomography (11C PiB-PET) data. 120 groups of PiB-PET images from the ADNI database were analyzed. The results showed that the small-world property of MCI and AD were lost as compared to HC. Furthermore, the local clustering of networks was higher in both MCI and AD as compared to HC, whereas the path length was similar among the three groups. The results also showed that there could be four potential A $\beta$  toxic oligomer seeds: Frontal\_Sup\_Medial\_L, Parietal\_Inf\_L, Frontal\_Med\_Orb\_R, and Parietal\_Inf\_R. These four seeds are corresponding to Regions of Interests referred by physicians to clinically diagnose AD.

**Keywords:** Alzheimer's disease, amyloid- $\beta$  peptide (A $\beta$ ), carbon 11-labeled pittsburgh compound B (11C-PiB), positron emission tomography (PET), brain networks

## 1. Introduction

Alzheimer's disease (AD) is one of the most common dementia diseases, and as such, it has swiftly become a serious health problem for aging populations around the world. Moreover, the main pathological feature of AD is the amyloid- $\beta$  peptide (A $\beta$ ) mechanism. In this mechanism, A $\beta$  plaques are generated and deposited in neural cells due to a gene mutation in the Beta Amyloid Precursor Protein and Presenilin. Consequently, an accumulation of these plaques results in brain oxidative

---

<sup>1</sup> The Project is sponsored by SRF for ROCS, SEM, and the Shanghai Excellent Young Teachers Program.

<sup>2</sup> Data used in preparation of this article were obtained from the Alzheimer's disease Neuroimaging Initiative (ADNI) database (adni.loni.usc.edu). As such, the investigators within the ADNI contributed to the design and implementation of ADNI and/or provided data but did not participate in analysis or writing of this report. A complete listing of ADNI investigators can be found at: [http://adni.loni.usc.edu/wp-content/uploads/how\\_to\\_apply/ADNI\\_Acknowledgement\\_List.pdf](http://adni.loni.usc.edu/wp-content/uploads/how_to_apply/ADNI_Acknowledgement_List.pdf).

\* Address for correspondence: Zhihua Yu, Shanghai Geriatric Institute of Chinese Medicine, No. 365, Xiangyang Nan Road, Shanghai, China. Tel.: 021-64720010; Fax: 021-64720010; E-mail: yzh1109@hotmail.com.

stress and vascular barrier and, eventually, in damaged white matter and neural cell death. In particular, the generation of toxic oligomers during the aggregation of the amyloid- $\beta$  (A $\beta$ ) peptides into amyloid fibrils and plaques has emerged as a central feature in the onset and progression of AD [1, 2]. However, the pattern of beta toxic oligomers' diffusion in human brains *in vivo* is unknown due to a lack of real-time functional imaging techniques at the cellular and fiber level [3].

The A $\beta$  mechanism is commonly explored by employing the functional imaging technique, carbon 11-labeled Pittsburgh compound B (11C-PiB) Positron emission tomography (PET) imaging. Moreover, 11C-PiB can specifically bind to A $\beta$  deposition in human brains and provides quantitative information on A $\beta$  burden *in vivo* [4, 5]. Although the transmission of toxic oligomers at the cellular level cannot be recorded by 11C-PiB-PET images in real-time, it is possible to hypothesize a diffusion model by deep-learning from a huge quantity of PiB-PET images with statistical methods.

Brain network analysis based on graph theory, which provides a mathematic model for discovering the structural and functional connections of cells and fibers in human brains, has been a popular issue in the neuroscience field in recent years [6, 7]. It is widely applied to the exploration of neurological diseases, such as AD, Schizophrenia, and Attention deficit and hyperactivity disorder (ADHD), by analyzing neural images like MEG, DTI, MRI, fMRI, and FDG-PET. However, this method has not yet been applied to the analysis of PiB-PET images.

This study centers on two main objectives: (1) to explore whether the brain network analysis based on graph theory method can be used to analyze PiB-PET images and to verify the physiological significance of A $\beta$  brain networks, and (2) if (1) is verified, to identify the functional hubs of the A $\beta$  brain networks. These hubs can be assumed as A $\beta$  toxic oligomer seeds in the A $\beta$  mechanism.

## 2. Materials and methods

### 2.1. Subjects

120 groups of PiB PET Data used in the preparation of this article were obtained from the Alzheimer's disease Neuroimaging Initiative (ADNI) database (adni.loni.usc.edu). The ADNI was launched in 2003 as a public-private partnership, led by Principal Investigator Michael W. Weiner, MD. The primary goal of ADNI has been to test whether serial magnetic resonance imaging (MRI), positron emission tomography (PET), other biological markers, and clinical and neuropsychological

Table 1  
Basic information of the 120 groups of PiB-PET images

Groups	AD (N=16)	MCI (N=67)	HC (N=37)	P-value		
				AD vs MCI	AD vs HC	MCI vs HC
Gender (M/F)	8F 8M	13F 54M	17F 20M	0.93 <sup>b</sup>	0.445 <sup>b</sup>	0.242 <sup>b</sup>
Age (years)	74.7±12.8	75.5±7.3	76.8±6.9	0.004 <sup>a,**</sup>	0.01 <sup>b,*</sup>	0.002 <sup>a,*</sup>
Weight (kg)	76.0±16.8	77.7±14.3	74.7±14.2	0.541 <sup>a</sup>	0.711 <sup>a</sup>	0.197 <sup>a</sup>
MMSE score	21.5±2.53	26.0±3.6	28.4±1.3	<0.001 <sup>a,**</sup>	<0.001 <sup>a,**</sup>	<0.001 <sup>a,**</sup>
CDR value	0.93±0.36	0.66±0.46	0.15±0.42	<0.001 <sup>a,**</sup>	<0.001 <sup>a,**</sup>	<0.001 <sup>a,**</sup>

Note: Data is presented as the mean  $\pm$  standard deviation.

AD, Alzheimer's disease; HC, healthy control; MCI, Mild Cognitive Impairment; MMSE, Mini mental state examination; CDR, Clinical Dementia Rating; F, females; M, males.

<sup>a</sup> P-value was obtained by the two-sample two-tailed t-test. <sup>b</sup> P-value was obtained by the two-tailed Pearson X<sup>2</sup> test. \* P-value is less than 0.05. \*\* P-value is less than 0.001.

assessment can be combined to measure the progression of mild cognitive impairment (MCI) and early Alzheimer's disease (AD). All of the images were in the Digital Imaging and Communications in Medicine (DICOM) format. Furthermore, the participants' enrollment was conditional based upon certain eligibility criteria, and the general inclusion/exclusion criteria may be found in Table 1.

## 2.2. PET image pre-processing

The imaging data was pre-processed by using Statistical Parametric Mapping 8 (SPM8) implemented in Matlab2014a. Each PET image was registered to the Montreal Neurological Institute (MNI, McGill University, Montreal, Canada) space. Then, they were normalized according to its window width  $W$  and window level  $L$ . Finally, the images were transferred to gray level images with a grayscale of [0, 255].

## 2.3. Brain regions extraction and normalization

Standardized AAL (automated anatomical labeling) brain anatomy marker template in SPM8 [8] (total of 90 brain regions with 45 regions in each hemisphere) was used to extract the brain regions. All of the images were divided into 90 nodes (one region as one node), and the average pixel value of each region was calculated as node values. Moreover, to eliminate differences among the individual images, every node value was normalized by subtracting the average pixel value of images.

## 2.4. Constructing the brain network

In this research, graph theory is used to construct the brain network. 90 AAL brain regions were considered as nodes. As the statistical method most frequently employed in analyzing the brain networks of medical images [6, 9, 10], the Pearson correlation method was used to calculate the interregional correlation coefficient, as is shown in Eq. (1):

$$r = \frac{1}{n-1} \sum_{i=1}^n \left( \frac{X_i - \bar{X}}{S_x} \right) \left( \frac{Y_i - \bar{Y}}{S_y} \right) \quad (1)$$

where  $r$  refers to the Pearson correlation coefficient, and  $n$  refers to the number of participants in each group (in this paper,  $n$  is 16 for AD, 67 for MCI, and 37 for HC). Furthermore,  $\bar{X}$  and  $\bar{Y}$  refer to the mean values of each of the two nodes, and  $S_x$  and  $S_y$  refers to the standard deviations of nodes  $X_i$  and  $Y_i$ , respectively.

Figure 1 shows three Pearson correlation matrices (90\*90) with AD, MCI, and HC data. To analyze above connectivity matrix, the density threshold method was used. According to [10], the density threshold range  $15\% \leq D \leq 50\%$  was chosen with an interval of 1%.

## 2.5. Network analysis

Four fundamental network parameters were used in this study: the clustering coefficient,  $C$ ; characteristic path length,  $L$ ; small world index,  $\sigma$ ; and betweenness centrality of nodes,  $B_i$ . The parameters were calculated by the open toolkit, The Brain Connectivity Toolbox (BCT,

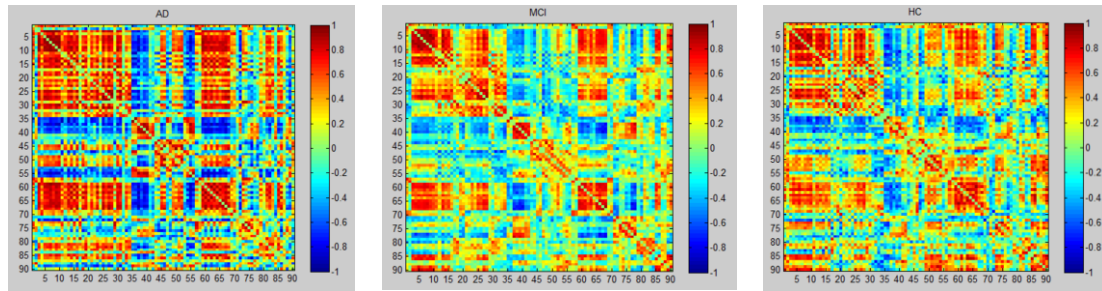


Fig. 1. Three correlation matrices obtained from Pearson correlation coefficients (indicated by color bar, ranging from -1.0 to 1.0) between 90 regions of interests controlled for age. From left to right: AD group, MCI group, and HC group.

<http://www.nitrc.org/projects/bct/>). The clustering coefficient  $C_i$  of node  $i$  indicates the degree to which the nodes in a graph tend to cluster together, and  $C$  is the average  $C_i$  value from all the nodes in the network. The characteristic path length  $L$  is defined as the average number of steps along the shortest paths for all possible pairs of network nodes. It is a measure of the efficiency of information or mass transport on a network [11]. Furthermore, the small world index  $\sigma$  presents the small-world property of brain network. Normally, a brain network has small world property when  $\sigma > 1$ . The  $\sigma$  was calculated by Eq. (2):

$$\sigma = \left( \frac{C/C_{rand}}{L/L_{rand}} \right) \quad (2)$$

where  $L_{rand}$  and  $C_{rand}$  refer to the corresponding random network path length and clustering coefficient, respectively. In this study, random networks were repeated 50 times in order to calculate  $\sigma$ .

Finally, the betweenness centrality  $B_i$  is an indicator of a node's (node  $i$ ) centrality in a network, and it is equal to the number of shortest paths from all vertices to all others that pass through node  $i$ .  $B_i$  is normally used to determine the candidate hubs in a network. In this study, the normalized parameter  $bi$  was defined by  $bi = B_i / \text{averaged } B_i$ . According to [11], all nodes with high  $bi$  values ( $> 1.5$  in HC, MCI, or AD groups) were considered as candidate hubs of the A $\beta$  brain networks. To calculate  $bi$ , a fixed density was determined by including all 90 nodes with minimal false-positive paths [12]. Finally, a density of 43% was chosen as the suitable density threshold in the present study.

## 2.6. Statistical analysis

To test differences of parameters among three diagnostic groups, a nonparametric permutation test was used [6]. Using the randomization procedure, each participant's node values were randomly reassigned, and the interregional correlation matrix was calculated again; additionally, a set of binary matrices was also obtained over the same density threshold range. Then  $C$ ,  $L$ ,  $\sigma$ , and  $bi$  at certain sparsities were computed separately for the three diagnostic groups. In this research, the whole procedure was repeated 500 times.

## 3. Results

### 3.1. The clustering coefficients $C$ and characteristic path length $L$

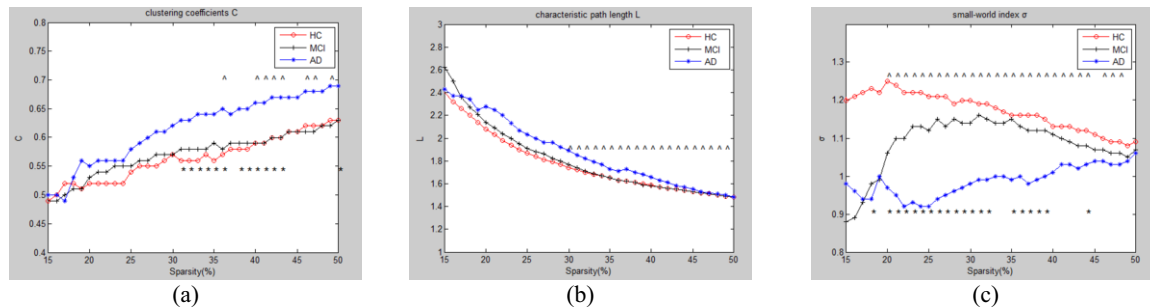


Fig. 2. Results of clustering coefficients  $C$ , characteristic path length  $L$ , and small-world index  $\sigma$  in the three groups. (a) The clustering coefficients  $C$ , (b) The characteristic path length  $L$ , and (c) The small-world index  $\sigma$  in the HC (red line), MCI (black line), and AD (blue line) groups. \* $p < 0.05$  for HC vs AD; ^ $p < 0.05$  for MCI vs AD.

The results of the clustering coefficients  $C$  and characteristic path length  $L$  for the three diagnostic groups (AD, MCI, and HC) are given in Figure 2. In Figure 2(a), the clustering coefficients  $C$  increase with increasing density. Furthermore, the density changes only slightly from group to group (15%~19%). In addition, the AD group has the highest  $C$  values, whereas the HC group has the lowest  $C$  values over a wide density range (20%~39%). For a density of 40%~50%, the AD group again has the highest  $C$  values; however, the MCI group has  $C$  values near those of the HC group. Furthermore, statistical analysis revealed that there are significant differences between the AD and HC groups at densities of 31%~36%, 38%~43%, and 50%, as well as significant differences between MCI and AD at densities of 40%~43%, 36%, 46%, 47%, and 49% ( $p < 0.05$ ).

In contrast to the clustering coefficients, it can be seen from Figure 2(b) that the characteristic path length  $L$  decreases with increasing density. Moreover, there are only slight differences among the three diagnostic groups. For example, when the density is 0.17, the  $L$  values of AD, MCI, and HC are 2.37, 2.36, and 2.26 respectively. Statistical analysis revealed that there is a significant difference between the AD and MCI groups at a density of 30% ~ 49% ( $p < 0.05$ ).

### 3.2. Small world index

Figure 2(c) exhibits the small world indexes of the three groups. It can be seen that for the HC group, the  $\sigma$  value is greater than 1 at all densities. As for the MCI group,  $\sigma$  is greater than 1 at a density of 20% ~ 50%, but  $\sigma$  is less than 1 at the other densities. However, for the AD group,  $\sigma$  is less than 1 at most densities. Statistical analysis revealed that there are significant differences between the AD and HC groups at densities of 20%~32%, 35%~39%, 18%, and 44%, as well as significant differences between MCI and AD at densities of 20%~44% and 46%~48% ( $p < 0.05$ ).

### 3.3. Functional hubs

Table 2 lists all of the  $bi$  values in the 90 brain regions of the 120 subjects in the three diagnostic groups. Figure 3 shows the related alterations in the hub regions. As a result, four particular regions, the Frontal\_Sup\_Medial\_L and Parietal\_Inf\_L of the left hemisphere as well as the Frontal\_Med\_Orb\_R and Parietal\_Inf\_R of the right hemisphere, were identified as functional candidate hubs in the process of network information transmission (AD&MCI>HC). They are potentially A $\beta$  toxic oligomer seeds in brains.

Table 2

The *bi* results of 90 brain regions in the 3 diagnostic groups (*n* refers to the sample number of each group)

<i>Brain regions</i>	<i>HC</i> ( <i>n</i> =37)	<i>MCI</i> ( <i>n</i> =67)	<i>AD (n=16)</i>	<i>Brain regions</i>	<i>HC</i> ( <i>n</i> =37)	<i>MCI</i> ( <i>n</i> =67)	<i>AD</i> ( <i>n</i> =16)
Precentral_L	0.51	0.85	0.79	Cuneus_R	0.85	0.85	0.77
Precentral_R	0.98	0.12	0.66	Lingual_L	1.42	1.51	0.18
Frontal_Sup_L	0.88	0.96	0.91	Lingual_R	0.51	0.69	0.99
Frontal_Sup_R	0.62	0.95	1.17	Occipital_Sup_L	0.61	1.19	0.75
Frontal_Sup_Orb_L	1.50	1.14	0.73	Occipital_Sup_R	1.03	0.78	0.55
Frontal_Sup_Orb_R	1.39	0.81	1.07	Occipital_Mid_L	2.14	0.09	0.31
Frontal_Mid_L	1.17	0.93	1.05	Occipital_Mid_R	1.06	0.69	0.44
Frontal_Mid_R	1.38	1.49	1.34	Occipital_Inf_L	0.77	0.99	0.67
Frontal_Mid_Orb_L	1.51	0.97	0.82	Occipital_Inf_R	1.41	0.84	1.29
Frontal_Mid_Orb_R	1.73	0.73	0.70	Fusiform_L	0.64	0.54	1.46
Frontal_Inf_Oper_L	1.40	0.95	1.12	Fusiform_R	1.12	1.20	2.05
Frontal_Inf_Oper_R	1.03	0.83	0.09	Postcentral_L	0.42	0.76	0.60
Frontal_Inf_Tri_L	2.05	1.12	0.88	Postcentral_R	0.27	0.69	0.68
Frontal_Inf_Tri_R	1.83	0.88	0.52	Parietal_Sup_L	1.54	1.44	1.93
Frontal_Inf_Orb_L	1.23	0.85	1.87	Parietal_Sup_R	1.58	1.11	0.92
Frontal_Inf_Orb_R	1.09	0.77	0.78	Parietal_Inf_L	<b>1.22</b>	<b>1.64</b>	<b>1.70</b>
Rolandic_Oper_L	0.61	0.55	1.64	Parietal_Inf_R	<b>0.55</b>	<b>1.62</b>	<b>1.74</b>
Rolandic_Oper_R	0.28	0.41	0.48	SupraMarginal_L	1.37	0.73	1.21
Supp_Motor_Area_L	0.27	0.94	1.56	SupraMarginal_R	1.19	0.94	1.03
Supp_Motor_Area_R	0.67	0.92	1.15	Angular_L	1.59	1.13	0.81
Olfactory_L	0.42	2.06	0.21	Angular_R	0.92	1.23	1.30
Olfactory_R	0.73	1.03	0.36	Precuneus_L	1.23	1.48	2.05
Frontal_Sup_MedialL	<b>0.36</b>	<b>1.57</b>	<b>1.58</b>	Precuneus_R	0.74	1.41	1.71
Frontal_Sup_MedialR	0.78	0.71	1.15	Paracentral_LobulL	0.91	0.29	0.50
Frontal_Med_Orb_L	0.86	1.64	1.01	Paracentral_LobulR	0.78	0.66	0.84
Frontal_Med_Orb_R	<b>1.08</b>	<b>3.35</b>	<b>2.14</b>	Caudate_L	0.20	1.99	0.06
Rectus_L	1.19	0.75	1.28	Caudate_R	1.28	0.82	0.47
Rectus_R	1.20	1.41	1.55	Putamen_L	1.52	0.18	0.70
Insula_L	0.56	0.26	0.46	Putamen_R	1.16	0.59	0.62
Insula_R	0.45	1.14	0.96	Pallidum_L	2.03	0.32	1.02
Cingulum_Ant_L	0.83	1.88	1.40	Pallidum_R	0.09	0.67	2.03
Cingulum_Ant_R	1.34	2.52	0.27	Thalamus_L	1.12	0.85	0.86
Cingulum_Mid_L	1.46	0.69	4.21	Thalamus_R	0.80	1.14	0.65
Cingulum_Mid_R	0.99	1.24	1.10	Heschl_L	0.07	0.15	0.43
Cingulum_Post_L	1.01	0.77	0.84	Heschl_R	0.20	2.22	0.24
Cingulum_Post_R	0.80	1.08	1.01	Temporal_Sup_L	1.17	0.79	0.64
Hippocampus_L	1.10	1.64	0.89	Temporal_Sup_R	1.29	0.87	1.85
Hippocampus_R	1.19	1.02	2.04	Temporal_PoleSupL	0.65	0.51	0.58
ParaHippocampal_L	1.95	1.45	1.11	Temporal_PoleSupR	0.98	1.20	0.68
ParaHippocampal_R	1.79	1.59	2.71	Temporal_Mid_L	1.17	1.21	0.79
Amygdala_L	0.63	0.90	0.03	Temporal_Mid_R	1.50	0.72	0.95
Amygdala_R	0.13	0.78	0.42	Temporal_PoleMiL	1.06	0.36	0.01
Calcarine_L	1.40	0.59	0.49	Temporal_PoleMiR	0.76	0.40	0.51
Calcarine_R	0.19	0.45	0.98	Temporal_Inf_L	0.98	1.42	1.14
Cuneus_L	0.03	0.24	1.05	Temporal_Inf_R	1.49	1.19	0.66

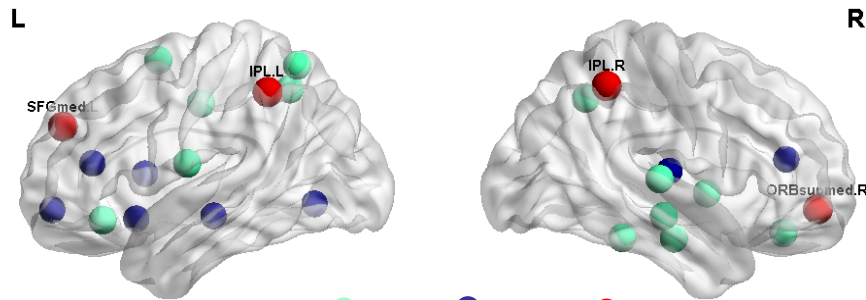


Fig. 3. Results of related alterations in hub regions. ● AD>HC; ● MCI>HC; ● AD&MCI>HC. The results were visualized by *BrainNet Viewer*.

#### 4. Discussion and conclusion

- The results demonstrated that in Aβ functional brain networks, the HC group has a small world property ( $\sigma > 1$ ), and this property decreases through the course of AD (HC>MCI>AD). These results are similar to results from other brain network analyses that were based on other functional imaging analyses [6, 7, 10]. This means Aβ functional brain networks have physiological significance.
- The results revealed that the Frontal\_Sup\_Medial\_L, Parietal\_Inf\_L, Frontal\_Med\_Orb\_R, and Parietal\_Inf\_R are AD- and MCI-related alterations in Aβ functional brain networks. Moreover, these four regions are potentially Aβ toxic oligomer seeds in brains. It is important to note that these four regions are similar to results claimed in previous medical literatures [4, 5], and these four regions are also ROIs referred by physicians to clinically diagnose AD [4]. Table 3 lists comparisons between the findings of the present study and findings from previous literature.

Table 3

Comparison between findings in the present study and literature

Objectives	Findings in this paper	Image approaches in literature (samples)	Findings in Literature	Comparison
Small-world property among the AD, MCI and HC groups	The HC group has small world property, which decreases through the course of AD (HC>MCI>AD). (HC=37, MCI=67, AD=16)	FDG-PET images (HC=94, MCI=183, AD=216)	<i>“The overall small-world property as seen in the CN whole brain network was preserved in MCI and AD (HC&gt;MCI&gt;AD)”</i> [6].	The transformation of the small world property during the course of AD is similar in the three different image approaches.
		fMRI images (HC=14, MCI=15, AD=12)	<i>“Small-worldness were significantly lower in aMCI and AD compared to NC in both low and high parcellation scales (HC&gt;aMCI &amp; AD)”</i> [10].	
Definition of ROIs (Aβ seeds) in clinics	Four ROIs (Frontal_Sup_Medial_L, Parietal_Inf_L, Frontal_Med_Orb_R, and Parietal_Inf_R) that are AD- and MCI-related alterations (AD&MCI>HC).	PiB-PET images (HC=5, MCI=5, AD=5)	5 anatomical brain areas are identified as Aβ ROIs, including PCG, PAR, FRT, LTC, and CAU [4].	The findings of this paper are the same or close to results from literature from the brain anatomy viewpoint.
		PiB-PET images (HC=15, AD=11)	11 ROIs are identified as Aβ ROIs, including CER, SWM, PON, CAU, SMC, FRT, PCG, LTC, MTC, and OCC [5].	

## Acknowledgements

Data collection and sharing for this project was funded by the Alzheimer's Disease Neuroimaging Initiative (ADNI) (National Institutes of Health Grant U01 AG024904) and DOD ADNI (Department of Defense award number W81XWH-12-2-0012). ADNI is funded by the National Institute on Aging, the National Institute of Biomedical Imaging and Bioengineering, and through generous contributions from the following: AbbVie, Alzheimer's Association; Alzheimer's Drug Discovery Foundation; Araclon Biotech; BioClinica, Inc.; Biogen; Bristol-Myers Squibb Company; CereSpir, Inc.; Eisai Inc.; Elan Pharmaceuticals, Inc.; Eli Lilly and Company; EuroImmun; F. Hoffmann-La Roche Ltd and its affiliated company Genentech, Inc.; Fujirebio; GE Healthcare; IXICO Ltd.; Janssen Alzheimer Immunotherapy Research & Development, LLC.; Johnson & Johnson Pharmaceutical Research & Development LLC.; Lumosity; Lundbeck; Merck & Co., Inc.; Meso Scale Diagnostics, LLC.; NeuroRx Research; Neurotrack Technologies; Novartis Pharmaceuticals Corporation; Pfizer Inc.; Piramal Imaging; Servier; Takeda Pharmaceutical Company; and Transition Therapeutics. The Canadian Institutes of Health Research is providing funds to support ADNI clinical sites in Canada. Private sector contributions are facilitated by the Foundation for the National Institutes of Health ([www.fnih.org](http://www.fnih.org)). The grantee organization is the Northern California Institute for Research and Education, and the study is coordinated by the Alzheimer's Disease Cooperative Study at the University of California, San Diego. ADNI data are disseminated by the Laboratory for Neuro Imaging at the University of Southern California.

## References

- [1] B.V. Zlokovic, Neurovascular mechanisms of Alzheimer's neurodegeneration, *Trends in neurosciences* **28** (2005), 202-208.
- [2] P. Scheltens, Dementia: Mild cognitive impairment—amyloid and beyond, *Nature Reviews Neurology* **9** (2013), 493-495.
- [3] S.I. Cohen, S. Linse, L.M. Luheshi, E. Hellstrand, D.A. White, L. Rajah, D.E. Otzen, M. Vendruscolo, C.M. Dobson and T.P. Knowles, Proliferation of amyloid- $\beta$ 42 aggregates occurs through a secondary nucleation mechanism, *Proceedings of the National Academy of Sciences* **110** (2013), 9758-9763.
- [4] J.C. Price, W.E. Klunk, B.J. Lopresti, X. Lu, J.A. Hoge, S.K. Ziolko, D.P. Holt, C.C. Meltzer, S.T. DeKosky and C.A. Mathis, Kinetic modeling of amyloid binding in humans using PET imaging and Pittsburgh Compound-B, *Journal of Cerebral Blood Flow & Metabolism* **25** (2005), 1528-1547.
- [5] M.D. Ikonovic, W.E. Klunk, E.E. Abrahamson, C.A. Mathis, J.C. Price, N.D. Tsopelas, B.J. Lopresti, S. Ziolko, W. Bi and W.R. Paljug, Post-mortem correlates of in vivo PiB-PET amyloid imaging in a typical case of Alzheimer's disease, *Brain* **131** (2008), 1630-1645.
- [6] E.H. Seo, D.Y. Lee, J.-M. Lee, J.-S. Park, B.K. Sohn, D.S. Lee, Y.M. Choe and J.I. Woo, Whole-brain functional networks in cognitively normal, mild cognitive impairment, and Alzheimer's disease, *PloS One* **8** (2013), e53922.
- [7] Z. Dai, C. Yan, K. Li, Z. Wang, J. Wang, M. Cao, Q. Lin, N. Shu, M. Xia and Y. Bi, Identifying and mapping connectivity patterns of brain network hubs in Alzheimer's disease, *Cerebral Cortex* (2014), 1-20, doi: 10.1093/cercor/bhu246.
- [8] N. Tzourio-Mazoyer, B. Landeau, D. Papathanassiou, F. Crivello, O. Etard, N. Delcroix, B. Mazoyer and M. Joliot, Automated anatomical labeling of activations in SPM using a macroscopic anatomical parcellation of the MNI MRI single-subject brain, *Neuroimage* **15** (2002), 273-289.
- [9] R.L. Buckner, J. Sepulcre, T. Talukdar, F.M. Krienen, H. Liu, T. Hedden, J.R. Andrews-Hanna, R.A. Sperling and K.A. Johnson, Cortical hubs revealed by intrinsic functional connectivity: Mapping, assessment of stability, and relation to Alzheimer's disease, *The Journal of Neuroscience* **29** (2009), 1860-1873.
- [10] Y. Sun, Q. Yin, R. Fang, X. Yan, Y. Wang, A. Bezerianos, H. Tang, F. Miao and J. Sun, Disrupted functional brain connectivity and its association to structural connectivity in amnesic mild cognitive impairment and Alzheimer's disease, *PloS One* **9** (2014), e96505.

- [11] E. Bullmore and O. Sporns, Complex brain networks: Graph theoretical analysis of structural and functional systems, *Nature Reviews Neuroscience* **10** (2009), 186-198.
- [12] V. Latora and M. Marchiori, Efficient behavior of small-world networks, *Physical Review Letters* **87** (2001), 198701.